On the Treatment of Electric and Magnetic Loss in the Linear Bicharacteristic Scheme for Electromagnetics

by

John H. Beggs, *Member*, IEEE

NASA/GSFC
Code 567
Greenbelt, MD 20771

March 2000

Abstract

The upwind leapfrog or Linear Bicharacteristic Scheme (LBS) has previously been extended to treat lossy dielectric and magnetic materials. This paper examines different methodologies for treatment of the electric loss term in the Linear Bicharacteristic Scheme for computational electromagnetics. Several different treatments of the electric loss term using the LBS are explored and compared on one-dimensional model problems involving reflection from lossy dielectric materials on both uniform and nonuniform grids. Results using these LBS implementations are also compared with the FDTD method for convenience.

1 Introduction

Numerical solutions of the Euler equations in Computational Fluid Dynamics (CFD) have illustrated the importance of treating a hyperbolic system of partial differential equations with the theory of characteristics and in an upwind manner (as opposed to symmetrically in space). These two features provide the motivation to use the Linear Bicharacteristic Scheme (LBS), or the upwind leapfrog method, for the construction of many practical wave propagation algorithms. The upwind leapfrog method has a more compact stencil compared with a classical leapfrog method. Clustering the stencil around the characteristic enables high accuracy to be achieved with a low operation count in a fully discrete way. This leads to a more natural treatment of outer boundaries and material boundaries. The LBS treats the outer boundary condition naturally without nonreflecting approximations or matched layers. The interior point algorithm predicts the outgoing characteristic variables, and the algorithm only requires information about the incoming characteristic variables at the domain boundaries. Through knowledge of the wave propagation angle, the local coordinates can be rotated to align with the characteristics, at which the boundary condition becomes almost exact. Therefore, no extraneous boundary condition or matched layers are required, which can introduce errors into the solution. The LBS also offers a natural treatment of dielectric interfaces, without any extrapolation or interpolation of fields or material properties near material discontinuities.

The LBS was originally developed to improve unsteady solutions in computational acoustics and aeroacoustics [1]-[7]. It is a classical leapfrog algorithm, but is combined with upwind bias in the spatial derivatives. This approach preserves the time-reversibility of the leapfrog algorithm, which results in no dissipation, and it permits more flexibility by the ability to adopt a characteristic based method. The use of characteristic variables allows the LBS to treat the outer computational boundaries naturally using the exact compatibility equations. The LBS offers a central storage approach with lower dispersion than the Yee algorithm, plus it generalizes much easier to nonuniform grids. It has previously been applied to two and three-dimensional free-space electromagnetic propagation and scattering problems [3], [6], [7]. It has also recently been extended to treat lossy dielectric and magnetic materials [8].

The objective of this paper is to examine different methodologies for treatment of the electric loss term in an attempt to find an accurate and self-consistent implementation that also works for perfect conductors in the limit of high conductivity (i.e. $\sigma \rightarrow \infty$). The final goal is to develop an implementation that will allow for an accurate and efficient extension of this approach to two-

and three-dimensional problems. This is accomplished by examining several different implementations of the electric loss term and by testing these implementations on one-dimensional model problems on both uniform and non-uniform grids. Section 2 of this paper provides a basic introduction to the LBS and it develops the different implementations for the electric loss term using the LBS. Section 3 presents results for one-dimensional model problems and Section 4 provides concluding remarks.

2 Theory

Maxwell's equations for linear, homogeneous and lossy media in the one-dimensional TE case (taking $\partial/\partial y = \partial/\partial z = 0$) are

$$\frac{\partial E_y}{\partial t} = \frac{1}{\epsilon}\left(-\frac{\partial H_z}{\partial x} - \sigma E_y\right) \tag{1}$$

$$\frac{\partial H_z}{\partial t} = \frac{1}{\mu}\left(-\frac{\partial E_y}{\partial x} - \sigma^* H_z\right) \tag{2}$$

where σ, σ^* are electric and magnetic conductivities, respectively. Using the electric displacement $D = \epsilon E$ and making the substitution $c = 1/\sqrt{\mu\epsilon}$ gives

$$\frac{\partial D_y}{\partial t} + \frac{\partial H_z}{\partial x} + \frac{\sigma}{\epsilon} D_y = 0 \tag{3}$$

$$\frac{1}{c^2}\frac{\partial Hz}{\partial t} + \frac{\partial D_y}{\partial x} + \sigma^* \epsilon H_z = 0 \tag{4}$$

The idea for the LBS is to transform the dependent variables D_y and H_z to characteristic variables. The algorithm presented here is the simplest leapfrog scheme described by Iserles [9] combined with upwind bias, or simply, the Linear Bicharacteristic Scheme (LBS). To transform (3) and (4) into characteristic form, we first multiply (4) by c and then add and subtract from (3) to give

$$\frac{\partial\left(D_y + \frac{1}{c}H_z\right)}{\partial t} + c\frac{\partial\left(D_y + \frac{1}{c}H_z\right)}{\partial x} + \frac{\sigma}{\epsilon}D_y + \sigma^*\epsilon c H_z = 0 \tag{5}$$

$$\frac{\partial\left(D_y - \frac{1}{c}H_z\right)}{\partial t} - c\frac{\partial\left(D_y - \frac{1}{c}H_z\right)}{\partial x} + \frac{\sigma}{\epsilon}D_y - \sigma^*\epsilon c H_z = 0 \tag{6}$$

Now define

$$P = D_y - \frac{1}{c}H_z \tag{7}$$

to represent the left propagating solution and

$$Q = D_y + \frac{1}{c}H_z \tag{8}$$

to represent the right propagating solution. P and Q are otherwise known as the characteristic variables. Using these definitions, equations (5) and (6) can be rewritten as

$$\frac{\partial Q}{\partial t} + c\frac{\partial Q}{\partial x} + \frac{1}{2}\left(\frac{\sigma}{\epsilon} - \sigma^*\epsilon c^2\right)P + \frac{1}{2}\left(\frac{\sigma}{\epsilon} + \sigma^*\epsilon c^2\right)Q = 0 \tag{9}$$

$$\frac{\partial P}{\partial t} - c\frac{\partial P}{\partial x} + \frac{1}{2}\left(\frac{\sigma}{\epsilon} + \sigma^*\epsilon c^2\right)P + \frac{1}{2}\left(\frac{\sigma}{\epsilon} - \sigma^*\epsilon c^2\right)Q = 0 \tag{10}$$

It is convenient to define and store the following coefficients before the time-stepping begins

$$a = \frac{\sigma}{\epsilon} + \sigma^*\epsilon c^2 \tag{11}$$

$$b = \frac{\sigma}{\epsilon} - \sigma^*\epsilon c^2 \tag{12}$$

Equations (9) and (10) can be rewritten more simply as

$$\frac{\partial Q}{\partial t} + c\frac{\partial Q}{\partial x} + \frac{b}{2}P + \frac{a}{2}Q = 0 \tag{13}$$

$$\frac{\partial P}{\partial t} - c\frac{\partial P}{\partial x} + \frac{a}{2}P + \frac{b}{2}Q = 0 \tag{14}$$

To develop the discretized algorithm for a one-dimensional system, the stencils of Figure 1 are proposed for the LBS. To solve the wave propagation problem without introducing dissipation, it is necessary that the stencil have central symmetry so that the scheme employed is reversible in time [2]. The stencil in Figure 1a is used for a right propagating wave and the stencil in Figure 1b is used for a left propagating wave. The upwind bias nature of the stencils is thus clearly evident. References [1], [2], [5], [6] and [7] clearly show that the UL method is second-order accurate. Note that the last two terms in equations (13) and (14) represent the electric and magnetic loss (or source) terms. The goal of this paper is to determine the most accurate and efficient method of treating these terms. To that end, several different implementations for these source terms will now be developed.

2.1 Method A

The first method, denoted by Method A, is to index both loss terms at time level $n+1$, for a semi-implicit formulation. This method was the original method recently proposed in [8]. Using the stencils shown in Figure 1, the resulting finite difference equations for (13) and (14) are

$$\frac{\left(Q_i^{n+1} - Q_i^n\right) + \left(Q_{i-1}^n - Q_{i-1}^{n-1}\right)}{2\Delta t} + c\left(\frac{Q_i^n - Q_{i-1}^n}{\Delta x}\right) + \frac{b}{2}P_i^{n+1} + \frac{a}{2}Q_i^{n+1} = 0 \tag{15}$$

$$\frac{\left(P_i^{n+1} - P_i^n\right) + \left(P_{i+1}^n - P_{i+1}^{n-1}\right)}{2\Delta t} - c\left(\frac{P_{i+1}^n - P_i^n}{\Delta x}\right) + \frac{a}{2}P_i^{n+1} + \frac{b}{2}Q_i^{n+1} = 0 \tag{16}$$

Rearranging (15) and (16) gives

$$Q_i^{n+1} - Q_i^n + Q_{i-1}^n - Q_{i-1}^{n-1} + 2\nu\left(Q_i^n - Q_{i-1}^n\right) + b\Delta t P_i^{n+1} + a\Delta t Q_i^{n+1} = 0 \tag{17}$$

$$P_i^{n+1} - P_i^n + P_{i+1}^n - P_{i+1}^{n-1} - 2\nu\left(P_{i+1}^n - P_i^n\right) + a\Delta t P_i^{n+1} + b\Delta t Q_i^{n+1} = 0 \tag{18}$$

where $\nu = c\Delta t/\Delta x$ is the Courant number. Now, collecting common terms in (17) and putting the n and $n-1$ time indexed terms on the right hand side (with a similar development for (18)) gives

$$Q_i^{n+1} + \frac{b\Delta t}{(1+a\Delta t)} P_i^{n+1} = \left[Q_{i-1}^{n-1} + (1-2\nu)\left(Q_i^n - Q_{i-1}^n\right)\right]/(1+a\Delta t) \tag{19}$$

$$\frac{b\Delta t}{(1+a\Delta t)} Q_i^{n+1} + P_i^{n+1} = \left[P_{i+1}^{n+1} - (1-2\nu)\left(P_{i+1}^n - P_i^n\right)\right]/(1+a\Delta t) \tag{20}$$

The right side of these equations is the residual and can be rewritten as

$$R_1^n = \left[Q_{i-1}^{n-1} + (1-2\nu)\left(Q_i^n - Q_{i-1}^n\right)\right]/(1+a\Delta t) \tag{21}$$

$$R_2^n = \left[P_{i+1}^{n+1} - (1-2\nu)\left(P_{i+1}^n - P_i^n\right)\right]/(1+a\Delta t) \tag{22}$$

Now, in relation to equations (19) and (20), the following definitions are made

$$a_{11} = 1 \tag{23}$$

$$a_{12} = (b\Delta t)/(1+a\Delta t) \tag{24}$$

$$a_{21} = (b\Delta t)/(1+a\Delta t) \tag{25}$$

$$a_{22} = 1 \tag{26}$$

$$\bar{A} = \begin{bmatrix} a_{11} & a_{12} \\ a_{21} & a_{22} \end{bmatrix} \tag{27}$$

$$\bar{R} = \begin{bmatrix} R_1^n \\ R_2^n \end{bmatrix} \tag{28}$$

$$\bar{X} = \begin{bmatrix} Q_i^{n+1} \\ P_i^{n+1} \end{bmatrix} \tag{29}$$

The update equations (19) and (20) are now rewritten as

$$\bar{A}\bar{X} = \bar{R} \tag{30}$$

with a solution given by

$$\bar{X} = \bar{A}^{-1}\bar{R} \tag{31}$$

where

$$\bar{A}^{-1} = \frac{1}{d}\begin{bmatrix} a_{22} & -a_{12} \\ -a_{21} & a_{11} \end{bmatrix} \tag{32}$$

$$d = a_{11}a_{22} - a_{12}a_{21} \tag{33}$$

The final update equations are then

$$Q_i^{n+1} = \frac{1}{d}\left(a_{22}R_1^n - a_{12}R_2^n\right) \tag{34}$$

$$P_i^{n+1} = \frac{1}{d}\left(-a_{21}R_1^n + a_{11}R_2^n\right) \tag{35}$$

Note that no computational penalty is incurred by this matrix solution, since the a, b and matrix coefficients can be precomputed and stored before time stepping begins, thus increasing the efficiency of the method. Note that for a PEC as $\sigma \to \infty$, from (34) and (35), $Q_i^{n+1} = P_i^{n+1} = 0$, as required. For lossless ($\sigma = \sigma^* = 0$), homogeneous dielectric and magnetic materials, the update equations are simply

$$Q_i^{n+1} = Q_{i-1}^{n-1} + (1-2\nu)\left(Q_i^n - Q_{i-1}^n\right) \tag{36}$$

$$P_i^{n+1} = P_{i+1}^{n-1} - (1-2\nu)\left(P_{i+1}^n - P_i^n\right) \tag{37}$$

To implement the dielectric material interface boundary condition, consider the one-dimensional grid shown in Figure 2. The dielectric interface is located at grid point i, and the dielectric materials can be lossy. The characteristic variables at grid point i, P_i and Q_i, are split into four components P_1, Q_1, P_2 and Q_2. The terms P_1 and Q_1 exist just to the left of the material interface as shown in Figure 2. The remaining terms P_2 and Q_2 exist just to the right of the material interface. For material 1, equation (34) is used to predict the value for Q_1^{n+1} at the boundary and for material 2, equation (35) is used to predict the value for P_2^{n+1} at the boundary. Then the electromagnetic boundary conditions are used to solve for P_1^{n+1} and Q_2^{n+1} in terms of the "known" characteristic variables Q_1^{n+1} and P_2^{n+1}. To develop this procedure, the electromagnetic boundary conditions on the tangential field components are given by

$$E_{y1} = E_{y2} \Rightarrow \frac{D_{y1}}{\epsilon_1} = \frac{D_{y2}}{\epsilon_2} \tag{38}$$

$$H_{z1} = H_{z2} \tag{39}$$

For the right-going wave, substituting (38) and (39) into (8) gives

$$\begin{aligned} Q_1^{n+1} &= D_{y1}^{n+1} + \frac{1}{c_1}H_{z1}^{n+1} \\ &= \frac{\epsilon_1}{2\epsilon_2}\left(P_2^{n+1} + Q_2^{n+1}\right) + \frac{c_2}{2c_1}\left(Q_2^{n+1} - P_2^{n+1}\right) \end{aligned} \tag{40}$$

Similarly, substituting (38) and (39) into (7) yields

$$P_2^{n+1} = \frac{\epsilon_2}{2\epsilon_1}\left(P_1^{n+1} + Q_1^{n+1}\right) - \frac{c_1}{2c_2}\left(Q_1^{n+1} - P_1^{n+1}\right) \tag{41}$$

Since Q_1^{n+1} and P_2^{n+1} are known at the boundary point i, it is necessary to express Q_2^{n+1} and P_1^{n+1} in terms of these variables. Rearranging (40) and (41) gives

$$Q_2^{n+1} = T_2 Q_1^{n+1} + \Gamma_2 P_2^{n+1} \tag{42}$$

$$P_1^{n+1} = \Gamma_1 Q_1^{n+1} + T_1 P_2^{n+1} \tag{43}$$

where

$$\Gamma_1 = \left(\frac{c_1\epsilon_1 - c_2\epsilon_2}{c_2\epsilon_2 + c_1\epsilon_1}\right) \tag{44}$$

$$T_1 = \left(\frac{2c_2\epsilon_1}{c_2\epsilon_2 + c_1\epsilon_1}\right) \tag{45}$$

$$\Gamma_2 = \left(\frac{c_2\epsilon_2 - c_1\epsilon_1}{c_2\epsilon_2 + c_1\epsilon_1}\right) \tag{46}$$

$$T_2 = \left(\frac{2c_1\epsilon_2}{c_2\epsilon_2 + c_1\epsilon_1}\right) \tag{47}$$

From (42) it is clear that the right-going wave in material 2 is a sum of a transmitted portion of the right-going wave in material 1 plus a reflected portion of the left-going wave in material 2. A similar argument can be made for the left-going wave in region 1. In fact, the coefficients in (42) and (43) are very similar to the classical Fresnel reflection and transmission coefficients. Because this is a semi-implicit method, a matrix solution is required to calculate P and Q at each grid point. Special care needs to be taken when the LBS calculates the solution at grid points $i-1$ and $i+1$. At grid point $i-1$, the term P_{i+1}^n in (22) becomes P_1^n. At grid point i, the terms Q_i^n and P_i^n in (21) and (22) become Q_1^n and P_2^n, respectively. At grid point $i+1$, the term Q_{i-1}^n in (21) becomes Q_2^n. Rearranging equation (17) we have for grid point i,

$$(1 + a_1\Delta t)\, Q_1^{n+1} = Q_{i-1}^{n-1} + (1 - 2\nu)\left(Q_1^n - Q_{i-1}^n\right) - b_1\Delta t P_1^{n+1} \tag{48}$$

Since the term P_1^{n+1} is unknown, we use the boundary condition (43) to give

$$\left[1 + \frac{b_1\Delta t\,\Gamma_1}{1 + a_1\Delta t}\right] Q_1^{n+1} + \frac{b_1\Delta t\, T_1}{1 + a_1\Delta t} P_2^{n+1} = R_1^n \tag{49}$$

Now we define

$$R_1^n = \left[Q_{i-1}^{n-1} + (1 - 2\nu)\left(Q_1^n - Q_{i-1}^n\right)\right]/(1 + a_1\Delta t) \tag{50}$$

$$a_{11} = 1 + \frac{b_1\Delta t\,\Gamma_1}{1 + a_1\Delta t} \tag{51}$$

$$a_{12} = \frac{b_1\Delta t\, T_1}{1 + a_1\Delta t} \tag{52}$$

A similar development using (18) and (42) yields

$$\left(\frac{2b_2\Delta t\, T_2}{1 + a_2\Delta t}\right) Q_1^{n+1} + \left[1 + \frac{b_2\Delta t\,\Gamma_2}{1 + a_2\Delta t}\right] P_2^{n+1} = R_2^n \tag{53}$$

and we define

$$R_2^n = \left[P_{i+1}^{n-1} - (1-2\nu)\left(P_{i+1}^n - P_2^n\right)\right]/(1+a_2\Delta t) \tag{54}$$

$$a_{21} = \frac{b_2\Delta t\, T_2}{1+a_2\Delta t} \tag{55}$$

$$a_{22} = 1 + \frac{b_2\Delta t\, \Gamma_2}{1+a_2\Delta t} \tag{56}$$

The matrix equation now becomes

$$\begin{bmatrix} a_{11} & a_{12} \\ a_{21} & a_{22} \end{bmatrix} \begin{bmatrix} Q_1^{n+1} \\ P_2^{n+1} \end{bmatrix} = \begin{bmatrix} R_1^n \\ R_2^n \end{bmatrix} \tag{57}$$

The solution of this matrix equation is

$$Q_1^{n+1} = \frac{1}{d}\left(a_{22}R_1^n - a_{12}R_2^n\right) \tag{58}$$

$$P_2^{n+1} = \frac{1}{d}\left(-a_{21}R_1^n + a_{11}R_2^n\right) \tag{59}$$

where d is defined by (33). Once Q_1^{n+1} and P_2^{n+1} have been obtained, the boundary conditions in (42) and (43) are applied to update Q_2^{n+1} and P_1^{n+1}. For the perfect conductor, the appropriate boundary conditions are $Q_2^{n+1} = P_2^{n+1} = 0.0$ and $P_1^{n+1} = -Q_1^{n+1}$, where Q_1^{n+1} is predicted from (48).

2.2 Method B

Method B averages the loss terms at time levels n and $n+1$, which still results in a semi-implicit formulation. The update equations remain the same as shown in (34) and (35), but the following definitions are made

$$R_1^n = \left[Q_{i-1}^{n-1} + (1-2\nu)\left(Q_i^n - Q_{i-1}^n\right) - \frac{a\Delta t}{2}Q_i^n - \frac{b\Delta t}{2}P_i^n\right] \Big/ \left(1+\frac{a\Delta t}{2}\right) \tag{60}$$

$$R_2^n = \left[P_{i+1}^{n-1} - (1-2\nu)\left(P_{i+1}^n - P_i^n\right) - \frac{b\Delta t}{2}Q_i^n - \frac{a\Delta t}{2}P_i^n\right] \Big/ \left(1+\frac{a\Delta t}{2}\right) \tag{61}$$

$$a_{11} = 1 \tag{62}$$

$$a_{12} = \frac{b\Delta t}{(2+a\Delta t)} \tag{63}$$

$$a_{21} = \frac{b\Delta t}{(2+a\Delta t)} \tag{64}$$

$$a_{22} = 1 \tag{65}$$

and the solution proceeds as in Method A. A dielectric surface boundary condition can be developed for Method B in the same manner as that for Method A, but the details of that analysis are omitted for the sake of brevity.

2.3 Method C

Method C indexes the Q loss term at time level $n+1$ and the P loss term at time level n in (13). Similarly, in (14), the P loss term is indexed at $n+1$ and the Q loss term is indexed at n. This method is an explicit approach and avoids the matrix solution inherent with the semi-implicit Methods A and B. To that end, the follwing definitions are made:

$$R_1^n = Q_{i-1}^{n-1} + (1-2\nu)\left(Q_i^n - Q_{i-1}^n\right) - b\Delta t P_i^n \tag{66}$$

$$R_2^n = P_{i+1}^{n-1} - (1-2\nu)\left(P_{i+1}^n - P_i^n\right) - b\Delta t Q_i^n \tag{67}$$

The update equations are then

$$Q_i^{n+1} = R_1^n/(1+a\Delta t) \tag{68}$$

$$P_i^{n+1} = R_2^n/(1+a\Delta t) \tag{69}$$

The dielectric surface boundary condition is obtained by direct application of (42) and (43).

2.4 Method D

Method D indexes both Q and P loss terms in (13) and (14) at time level n, which is also an explicit approach. The residual terms become

$$R_1^n = Q_{i-1}^{n-1} + (1-2\nu)\left(Q_i^n - Q_{i-1}^n\right) - a\Delta t Q_i^n - b\Delta P_i^n \tag{70}$$

$$R_2^n = P_{i+1}^{n-1} - (1-2\nu)\left(P_{i+1}^n - P_i^n\right) - a\Delta t P_i^n - b\Delta t Q_i^n \tag{71}$$

and the update equations are

$$Q_i^{n+1} = R_1^n \tag{72}$$

$$P_i^{n+1} = R_2^n \tag{73}$$

Unfortunately, this method is unstable for long time integrations and for high conductivity values. As noted by Thomas [5], this is a straightforward application of the upwind leapfrog method to the loss (or source) terms in (13) and (14), which he showed to be unstable. He proposed an alternative method for one source term which stabilizes the algorithm, and these methods including variations are considered next. Since Method D is unstable, no numerical results will be presented using this implementation.

2.5 Method E

Method E relies upon the method proposed by Thomas [5] to stabilize the upwind leapfrog algorithm when source terms are present in the governing equations. The idea is to introduce a

transformation

$$Q = e^{-at/2}V \tag{74}$$

into (13) which gives (after some work)

$$\frac{\partial V}{\partial t} + c\frac{\partial V}{\partial x} + \frac{b}{2}e^{at/2}P = 0 \tag{75}$$

Applying a similar transformation

$$P = e^{-at/2}W \tag{76}$$

to (14) gives

$$\frac{\partial W}{\partial t} + c\frac{\partial W}{\partial x} + \frac{b}{2}e^{at/2}Q = 0 \tag{77}$$

Method E and the following two methods deal with treatment of the remaining source term in (75) and (77). For Method E, we index the source terms at time level $n+1$. Applying the stencils of Figure 1 to (75) and (77) and noting that

$$V_i^n = e^{an\Delta t/2}Q_i^n \tag{78}$$

$$W_i^n = e^{an\Delta t/2}P_i^n \tag{79}$$

gives the following equations

$$Q_i^{n+1} + b\Delta t P_i^{n+1} = R_1^n \tag{80}$$

$$b\Delta t Q_i^{n+1} + P_i^{n+1} = R_2^n \tag{81}$$

where

$$R_1^n = e^{-a\Delta t}Q_{i-1}^{n-1} + e^{-a\Delta t/2}(1-2\nu)\left(Q_i^n - Q_{i-1}^n\right) \tag{82}$$

$$R_2^n = e^{-a\Delta t}P_{i+1}^{n-1} - e^{-a\Delta t/2}(1-2\nu)\left(P_{i+1}^n - P_i^n\right) \tag{83}$$

Thomas [5] used a second order Taylor series expansion of the terms $e^{-a\Delta t}$ and $e^{a\Delta t}$ to derive the final update equations to avoid a costly exponential matrix evaluation and inversion. This is a concern especially for multidimensional applications and for multiple source terms. However, the Taylor series expansion is not implemented in the present context, since these exponential updating coefficients can be precomputed and stored before time stepping begins. No computational penalty is incurred by using the full exponential terms. The update equations are

$$Q_i^{n+1} = \frac{1}{d}\left(a_{22}R_1^n - a_{12}R_2^n\right) \tag{84}$$

$$P_i^{n+1} = \frac{1}{d}\left(-a_{21}R_1^n + a_{11}R_2^n\right) \tag{85}$$

with the following definitions

$$a_{11} = 1 \tag{86}$$

$$a_{12} = b\Delta t \tag{87}$$

$$a_{21} = b\Delta t \tag{88}$$

$$a_{22} = 1 \tag{89}$$

and d is given by (33). The dielectric surface boundary condition is similar to that for Method A. Unfortunately, this approach exhibits a late-time instability problem for lossy dielectric materials. A Taylor series expansion of the exponential terms proposed by Thomas [5] results in a slightly different scheme that also exhibits late time instability.

2.6 Method F

Method F is similar to Method E, but averages the source term in (75) and (77) between time levels $n+1$ and n. This results in the equations

$$R_1^n = e^{-a\Delta t}Q_{i-1}^{n-1} + e^{-a\Delta t/2}(1-2\nu)\left(Q_i^n - Q_{i-1}^n\right) - \frac{b\Delta t}{2}e^{-a\Delta t/2}P_i^n \tag{90}$$

$$R_2^n = e^{-a\Delta t}P_{i+1}^{n-1} - e^{-a\Delta t/2}(1-2\nu)\left(P_{i+1}^n - P_i^n\right) - \frac{b\Delta t}{2}e^{-a\Delta t/2}Q_i^n \tag{91}$$

and

$$a_{11} = 1 \tag{92}$$

$$a_{12} = b\Delta t/2 \tag{93}$$

$$a_{21} = b\Delta t/2 \tag{94}$$

$$a_{22} = 1 \tag{95}$$

The final update equations are the same as (84) and (85). Again, the dielectric surface boundary condition is similar to that in Method A. This method also suffers from a late time instability problem, although the instability growth is not quite as rapid as in Method E. An alternative scheme based on a Taylor series expansion of the exponential terms also exhibits late-time instability. Therefore, no results for Methods E and F will be presented.

2.7 Method G

The last method considered indexes the source term in (75) and (77) at time level n. This gives the final update equations as

$$Q_i^{n+1} = e^{-a\Delta t}Q_{i-1}^{n-1} + e^{-a\Delta t/2}(1-2\nu)\left(Q_i^n - Q_{i-1}^n\right) - b\Delta t e^{-a\Delta t/2}P_i^n \tag{96}$$

$$P_i^{n+1} = e^{-a\Delta t}P_{i+1}^{n-1} - e^{-a\Delta t/2}(1-2\nu)\left(P_{i+1}^n - P_i^n\right) - b\Delta t e^{-a\Delta t/2}Q_i^n \tag{97}$$

The dielectric surface boundary condition is obtained by a direct application of (42) and (43). This method is stable and does not exhibit any signs of late-time instability.

3 Results

The numerical results for this paper concentrate on one-dimensional model problems involving reflection from lossy dielectric materials on both uniform and nonuniform grids. The problem space size is 1000 cells with nonperiodic boundary conditions. For the uniform grid, a space step of 1 cm is used, the time step is 0.33 ps and the Courant number $\nu = 1$. For the boundary conditions, a Gaussian point source at $i = 0$ is used to specify $Q(0)$ and $P(1000) = 0$. For many complex geometries, it is often desirable to implement nonuniform grids to reduce the computational effort and memory resources and to improve modeling accuracy. We define a nonuniform grid by using a mesh stretch ratio of $M \equiv \Delta x_{max}/\Delta x_{min}$ which is periodic every 10 cells. Figure 3 shows an expanded view of a typical one-dimensional nonuniform grid with a mesh stretch ratio of 2 and a periodicity of 10 cells. The Courant number for a nonuniform grid is defined by $c\Delta t/\Delta x_{min}$, where Δx_{min} is the smallest cell size in the nonuniform grid.

The first problem is a reflection and transmission problem for a lossy dielectric half space on a nonuniform grid. The dielectric half space extends from $5 \leq x \leq 10$ with material parameters $\epsilon_{r2} = 10$, $\sigma_2 = 0.2$, $\sigma^* = 0$ and $\mu_{r2} = 1$. Figure 4 shows the reflection coefficient magnitude results for the exact solution, the FDTD method and the various LBS implementations calculated at $x = 4.0$ m (cell $i = 276$). Note that the FDTD results vary widely over the entire frequency band due to the nonuniform grid structure. However, most of the LBS implementations have comparable accuracy to the FDTD method, and these results are quite smooth, even for the nonuniform grid. Figure 5 shows the percent error in reflection coefficient magnitude for the LBS implementations. The FDTD method was not shown due to the wide variation in error. Note that Method C for the LBS implementations has the overall lowest error over the entire frequency range, and is therefore the method of choice for modeling lossy media with the LBS.

The second problem was the same as the previous case, but with a uniform grid of 1 cm spacing and material parameters $\epsilon_{r2} = 50$, $\sigma_2 = 0.2$, $\sigma^* = 0$ and $\mu_{r2} = 1$. Figure 6 shows the reflection coefficient magnitude results for the exact solution, the FDTD method and the various LBS implementations calculated at $x = 4.0$ m (cell $i = 401$). Note that the FDTD method exhibits slightly better agreement for lower frequencies, but then diverges sharply at higher frequencies. Figure 7 shows the percent error in reflection coefficient magnitude for the LBS implementations, which

maintain a rather flat frequency dependence at higher frequencies. This provides increased accuracy and fidelity for the higher frequency components in a given simulation. Although Method B exhibits slightly lower error at very low frequencies for this particular problem, the differences between methods is not significant enough to prefer Method B over any other method. Method C is the most suitable alternative for multidimensional applications.

The third problem was the same as the previous case, but with material parameters $\epsilon_{r2} = 80$, $\sigma_2 = 0.0$, $\sigma^* = 0$ and $\mu_{r2} = 1$. Figure 8 shows the reflection coefficient magnitude results for the exact solution, the FDTD method and the various LBS implementations calculated at $x = 5.0$ m (cell $i = 500$). Note that the FDTD method diverges sharply at higher frequencies, but the LBS methods are exact, and each LBS method reduces to the standard implementation for lossless dielectric media.

The final problem was also the same, but with a lossless magnetic media with material parameters $\epsilon_{r2} = 1$, $\sigma_2 = 0.0$, $\sigma^* = 0$ and $\mu_{r2} = 5000$. Figure 9 shows the reflection coefficient magnitude results for the exact solution, the FDTD method and the various LBS implementations calculated at $x = 5.0$ m (cell $i = 500$). Note how the FDTD method diverges from the exact solution, but the LBS methods are again exact for lossless magnetic media. Both the FDTD method and LBS methods had difficulty in predicting correct reflection coefficient results for lossy magnetic media, which could be the result of not updating the electric and magnetic conduction currents as separate solution variables. This alternative will be explored for further research.

4 Conclusions

This paper has examined seven implementations of the Linear Bicharacteristic scheme for computational electromagnetics to treat heterogeneous lossy dielectric and magnetic materials. Two of the six implementations exhibited late-time instabilities and were therefore eliminated from further consideration. The remaining four implementations were tested on simple one-dimensional model problems involving reflection from lossless and lossy dielectric and/or magnetic half-spaces. It was found that the method of choice involved indexing one source term at the present time level, and the coupled source term at the previous time level. This implementation provided two benefits. First, it provided similar or better accuracy than the other implementations. Second, it is the most suitable implementation for multi-dimensional problems to avoid a matrix solution at each time step. Overall, the LBS has several distinct advantages over conventional FDTD algorithms. First, the LBS is a second-order accurate algorithm which is about 2-3 times as eco-

nomical. The LBS can also be made to have zero dispersion error in certain instances. Second, the LBS provides a more natural and flexible way to implement surface boundary conditions and outer boundary conditions by using characteristics and an upwind bias technique popular in fluid dynamics. Third, the LBS provides more accurate results on nonuniform grids. The upwind biasing provides a more flexible generalization to unstructured grids. The results of this particular study and a previous study [8] indicate that the LBS is a superior algorithm for treatment of dielectric materials, especially its performance on nonuniform grids. Based on these results, the LBS is a very promising alternative to a conventional FDTD algorithm for many applications.

References

[1] J. P. Thomas and P. L. Roe, "Development of non-dissipative numerical schemes for computational aeroacoustics", vol. AIAA paper 93–3382CP, pp. 906–916, 1993.

[2] P. Roe, "Linear Bicharacteristic Schemes without dissipation", Tech. Rep. ICASE Report 94-65, ICASE, NASA Langley Research Center, 1994.

[3] B. Nguyen and P. Roe, "Application of an upwind leap-frog method for electromagnetics", in *Proc. 10th Annual Review of Progress in Applied Computational Electromagnetics*, Monterey, CA, March 1994, Applied Computational Electromagnetics Society, pp. 446–458.

[4] J. P. Thomas, C. Kim and P. Roe, "Progress toward a new computational scheme for aeroacoustics", in *AIAA 12th Computational Fluid Dynamics Conference*. AIAA, 1995.

[5] J. P. Thomas, *An Investigation of the Upwind Leapfrog Method for Scalar Advection and Acoustic/Aeroacoustic Wave Propagation Problems*, PhD thesis, University of Michigan, Ann Arbor, MI, 1996.

[6] B. Nguyen, *Investigation of Three-Level Finite-Difference Time-Domain Methods for Multidimensional Acoustics and Electromagnetics*, PhD thesis, University of Michigan, Ann Arbor, MI, 1996.

[7] C. Kim, *Multidimensional Upwind Leapfrog Schemes and Their Applications*, PhD thesis, University of Michigan, Ann Arbor, MI, 1997.

[8] J. H. Beggs and S. L. Chan, "The linear bicharacteristic scheme for computational electromagnetics", *IEEE Trans. Antennas Propag.*, 2000, submitted.

[9] A. Iserles, "Generalized leapfrog methods", *IMA Journal of Numerical Analysis*, vol. 6, pp. 381–392, 1986.

5 Figure Captions

Figure 1. One-dimensional upwind leapfrog computational stencils for right-going (a) and left-going (b) characteristics.

Figure 2. One-dimensional computational grid for the LBS showing characteristic variables, a dielectric interface located at cell i, and corresponding field components and characteristic variables used for the surface boundary condition.

Figure 3. Section of a one-dimensional non-uniform grid with a mesh stretch ratio of 2 and a base cell size of 1 cm. The grid variation is periodic every 10 cells.

Figure 5. Reflection coefficient magnitude versus frequency for reflection from a lossy dielectric half-space using the FDTD method and the LBS implementations on a non-uniform grid.

Figure 6. Percentage error in reflection coefficient magnitude versus frequency for reflection from a lossy dielectric half-space using the LBS implementations on a non-uniform grid.

Figure 7. Reflection coefficient magnitude versus frequency for reflection from a lossy dielectric half-space using FDTD and the LBS on a uniform grid.

Figure 8. Percentage error in reflection coefficient magnitude versus frequency for reflection from a lossy dielectric half-space using the LBS implementations on a uniform grid.

Figure 9. Reflection coefficient magnitude versus frequency for reflection from a lossless magnetic half-space using FDTD and the LBS on a uniform grid.

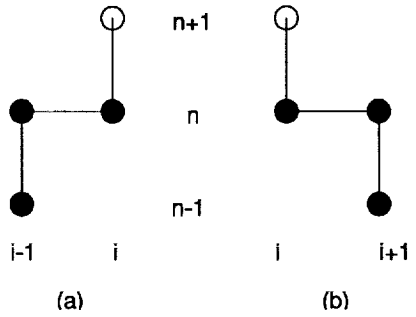

Figure 1:

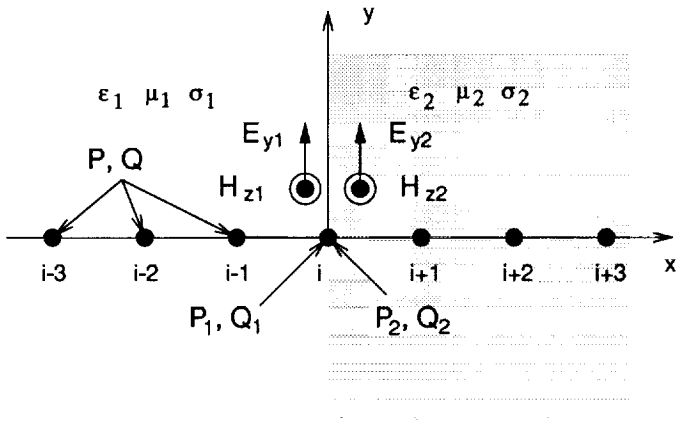

Figure 2:

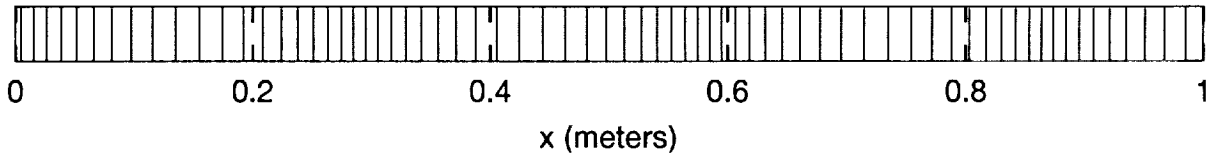

Figure 3:

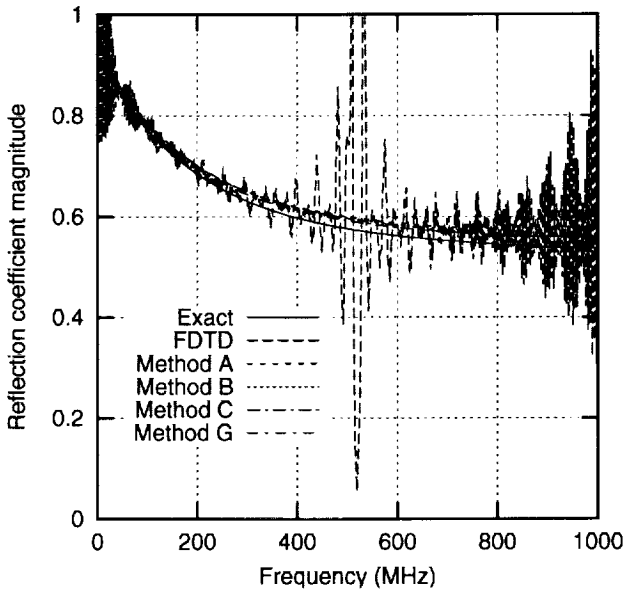

Figure 4:

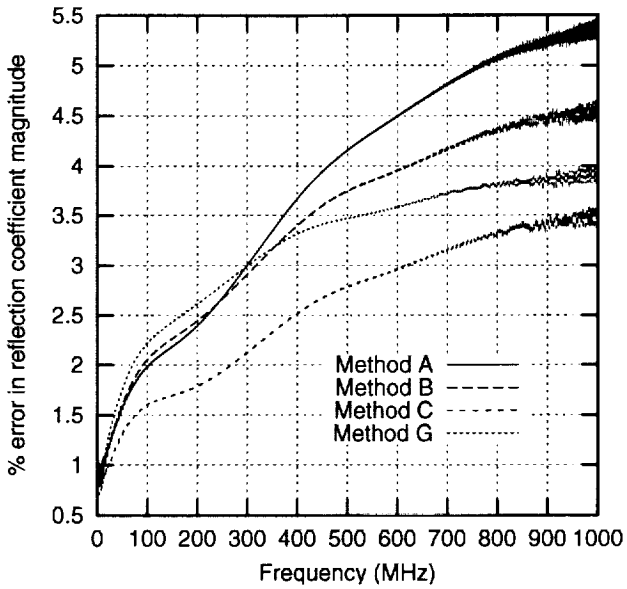

Figure 5:

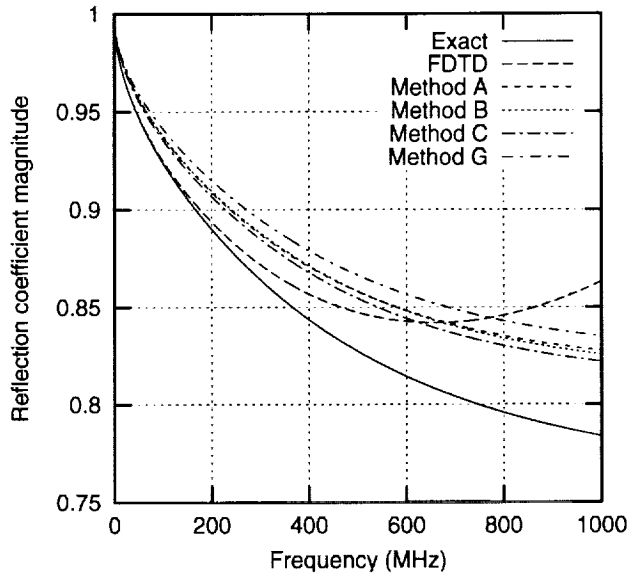

Figure 6:

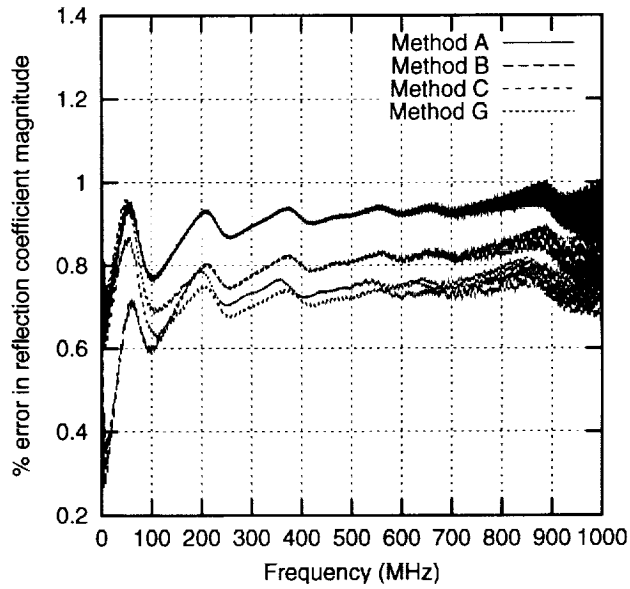

Figure 7:

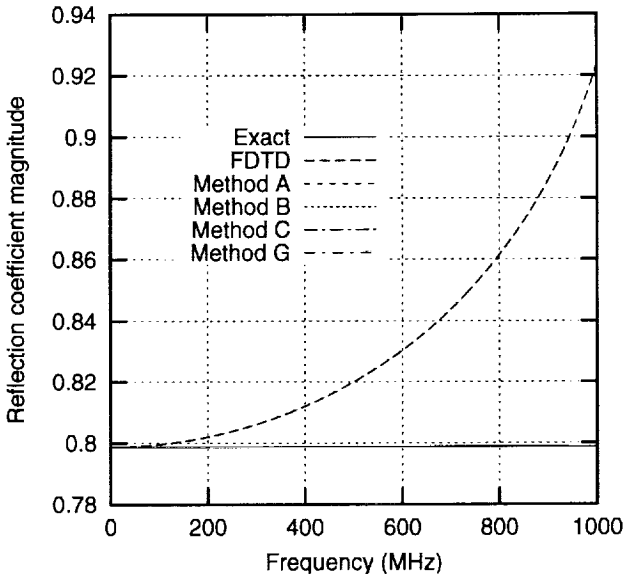

Figure 8:

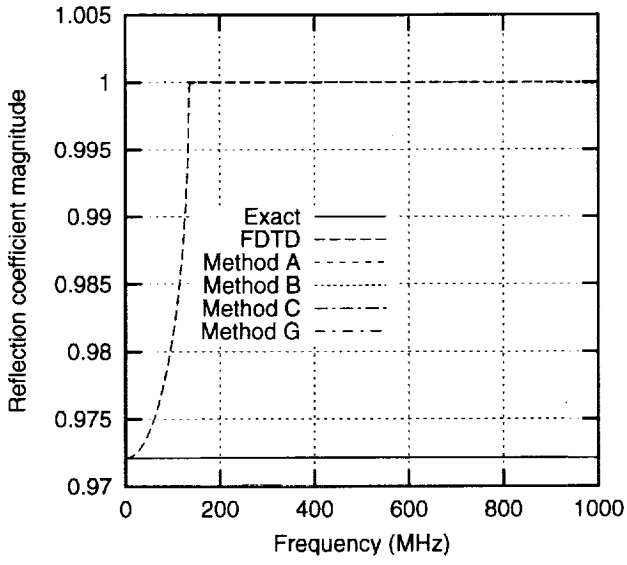

Figure 9: